Plasmonics
https://doi.org/10.1007/s11468-020-01267-8

A Hybrid Machine Learning Model to Study UV-Vis Spectra of Gold Nanospheres

B. Karlik[1] · M. F. Yilmaz[2] · M. Ozdemir[3] · C.T. Yavuz[4] · Y. Danisman[5]

Received: 29 April 2020 / Accepted: 18 August 2020

Abstract
Here, we have employed principal component analysis (PCA) and linear discriminant analysis (LDA) to analyze the Mie-calculated UV-Vis spectra of gold nanospheres (GNS). Eigen spectra of PCA perform the Fano-type resonances. PCA vector spectra determine the 3D vector fields which reveal the homoclinic orbit strange attractor. Quantum confinement effects are observed by the 3D representation of LDA. Standing wave patterns resulting from oscillations of ion-acoustic phonon and electron waves are illustrated through the eigen spectra of LDA. Such capabilities of GNPs have brought high attention to the high energy density physics applications. Furthermore, accurate prediction of gold nanoparticle (GNP) sizes using machine learning could provide rapid analysis without the need for expensive analysis. Two hybrid algorithms consist of unsupervised PCA and two different supervised ANN have been used to estimate the diameters of GNPs. PCA-based artificial neural networks(ANN) were found to estimate the diameters with a high accuracy.

Keywords Plasmonic nanoparticle · Plasmon spectra · Polariton · Fano resonance · Pattern recognition · Vector fields · Strange attractor · Artificial neural networks

Introduction

The arrangement of metal nanoparticles in an order of chain or array provides surface plasmon polaritons (SPPs), which are the bosonic (quasiparticles) coupled modes of an incident electromagnetic wave and free electrons (plasmon) of the surface. SPPs can manipulate the electromagnetic radiation and perform as micro-optical devices and can propagate in an undistorted manner for several diffraction lengths along a metal surface [1–3]. Fano resonance stands as the primary physical mechanism behind the manipulation of electromagnetic waves. Fano resonances are generated by the coupling of discrete excited states to a continuum of states and can be produced through the scattering of the electromagnetic waves by nano-particles [4, 5]. Furthermore, Semouchkina et al. showed that Fano-type shape and significant strength of the observed resonance are characteristic of the interaction of dielectric resonator arrays with the Fabry-Perot standing waves [6]. Besides, Sergeyev et al. proposed that spiral attractors generated by the interaction of dissipative solitons with carbon nanotubes are the main mechanisms that provide the trapping and manipulation of light [7]. Such capabilities of NPs brought the attention of application for high energy density physics. Kaymak et al. has shown that ultra-dense high energy density plasmas ($n_e > 9 \times 10^{24}$ cm^{-3}) can be generated by the irradiation of relativistic intensity femtosecond laser with aligned nanowires [8]. Ostrikov et al. proposed that several important properties of nanostructured targets are important for various applications such as the creation of dense hot plasmas at a temperature of 2–4 keV, efficient X-rays, and ion sources [9]. Lastly, Rocca et al. has justified that array-formatted nanowires completely absorb the high energy pulses and thereby produce an efficient number of neutrons

✉ M. F. Yilmaz

[1] Neurosurgical Simulation and Artificial Intelligence Learning Centre, Montreal Neurological Institute, McGill University, H3A2B4, Montreal, QC, Canada

[2] Independent Scholar, Fremont, USA

[3] Department of Basic Sciences and Humanities, College of Engineering, Imam Abdulrahman Bin Faisal University, P.O. Box 1982, Dammam 31451, Kingdom of Saudi Arabia

[4] Korea Advanced Institute of Science and Technology, 291 Daehak-ro, Yuseong-gu, Daejeon 34141, Republic of Korea

[5] Department of Mathematics and Computer Sciences, Queensborough Community College, CUNY, Bayside, New York, NY, USA

[10]. These capabilities of nanoparticles have strong impacts in the field of high energy density physics of fusion applications.

UV-vis spectroscopy as a useful tool is employed for the characterization, estimation of the sizes of nanoparticles, concentration, and aggregation level. It is a useful technique as UV-vis spectrometers can be found in many laboratories, the analysis does not change the sample, and the time needed for registration of the spectrum is very short. If the appropriate correction of the metal-dielectric constant for the nanoparticle size and the physicochemical environment is provided, then the Mie theory can be used to analyze the extinction spectra of AuNP recorded by UV-vis spectroscopy [10–12]. On the other hand, Yilmaz et al. has shown that the application of PCA and LDA (linear discriminant analysis) over the spectral database of plasma could inform more physical insight of deeper structures and polarization types of the ion species and electron-ion oscillations in the plasma [13, 14].

PCA and LDA are the two of the most common pattern recognition techniques that are used in order to reduce the dimensions of a given raw data in pattern recognition problems. PCA uses rotational transformation in a way that most of the data variability remains in a space of low dimensions, and it ignores the remaining dimensions that contain little variability. LDA, as a pattern recognition technique, is quite similar to that of PCA. The main difference is that LDA determines the vectors that best separate the classes while trying to keep the variance maximum. Although it looks like LDA outperforms PCA in multi-class settings where class labels are known, it might not always be the case, especially if the sizes of the classes in the data sets are relatively small. Besides, LDA performs well only if the classes have equal co-variance. PCA is good at keeping dimensions of highest variance, but it can disregard discriminant dimensions where LDA is needed. It is easy to find examples where LDA outperforms PCA and vice versa [13, 14].

Artificial neural network (ANN) algorithms have also been of great interest and employed in the last few decades for many applications such as remote sensing, computer vision, pattern recognition, and medical diagnosis. The ANN algorithms can easily identify and extract the patterns by setting a correlation between sets of given inputs and outputs through a training process. This adaptive nature makes them particularly appropriate for dealing with complex and non-linear problems. Another advantage of a machine learning algorithm is the fact that it can establish a strong correlation between the parameters without any knowledge of them. Therefore, it enables the handling of uncertainties, data with noise, and non-linear relationships which are hard to determine [15].

ANNs have been applied to both X-ray spectra to predict plasma electron temperatures and densities, and to UV-vis and FTIR spectra to investigate forensics [16, 17]. Lately, they have been used to estimate the diameters of nanoparticles [18, 19]. Peurifoy et al. have proposed artificial neural networks to approximate light scattering by multi-layer nanoparticles [20].

The selection of inputs is one of the most significant components of designing a classifier based on pattern recognition since even the best classifier does not work well unless the inputs are chosen very well. The complexity of the classifier method is inversely proportional to its classification efficiency. Recently, Karlik et al. has indicated the positive effects of hybrid learning methods consisting of unsupervised clustering and supervised classifiers [21]. So, in this work, a hybrid classifier consisting of an unsupervised PCA and a supervised ANN algorithm has been used. In this hybrid classifier, the input nodes of supervised ANN activations are derived through unsupervised PCA of the input data, which enables the neural system to deal with the statistics of the measurement error directly. Therefore, we have first employed the Mie scattering generated spectra of GNS as our database. This database was then analyzed by PCA and LDA methods, and the physical interpretations of PCA and LDA of UV-vis spectra of gold were examined. Then, the extracted PCA coordinates were used for the training of ANN to estimate the diameters of GNS. Finally, the experimental spectra of gold spheres with diameters 5, 7, 10, 15, 20, and 30 nm were tested for the estimation of diameters. Our findings reveal that the PCA-based artificial neural network (ANN) estimates the diameters of gold nanoparticles with a remarkably high accuracy.

Methods

Materials

Hydrogen tetrachloroaurate (III) trihydrate ($HAuCl_4.3H_2O$, gold salt), trisodium citrate (reducing agent), and sodium chloride were obtained from Aldrich and used as received. Gold nanoparticles (AuNPs) with the sizes of 5, 7, 10, 15, 20, and 30 nm (Fig.1) were purchased from Nanocomposix, Inc. Distilled water was used to prepare the aqueous solutions of AuNPs. Au nanoparticles were synthesized through the well-established reduction methods of Turkevich, Frens, and Jana [22–24]. In the preparation of 5 nm AuNPs, a 10 mL aqueous solution containing 0.25 mM $HAuCl_4$ and 0.25 mM trisodium citrate were first prepared. Ice-cooled 0.3 mL of 0.1 M sodium borohydride was added to this solution while stirring. The change in the color of the solution was an indicator of particle formation.

Synthesis

For the synthesis of 7 nm or larger AuNPs, aqueous solutions of 0.254 mM $HAuCl_4$ and 38.8 mM trisodium citrate

were first prepared. In a typical synthesis, 50 mL $HAuCl_4$ solution was heated to boiling. After 5 min, a 0.4–2.0 mL trisodium citrate solution was added to this mixture at once and the mixture was stirred for approximately 15 min. The color of the reaction mixture turned from yellow to colorless and then ruby red color depending on the AuNPs sizes. After cooling to RT, the samples were centrifuged and washed several times with DI water to obtain 5, 7, 10, 15, and 30 nm citrate-coated AuNPs.

Characterization

Dynamic light scattering (DLS, Malvern Zetasizer Nano ZS) technique was employed for the calculation of the average hydrodynamic diameters of gold nanoparticles. By using a He-Ne laser (4 mW) operated at 633 nm, Nano ZS detects the scattered light at an angle of 173°, which is known as backscatter detection. Aqueous 10 mM NaCl solutions were used in all DLS measurements.

Mie Scattering

The Mie theory describes the scattering of an electromagnetic wave by homogenous spherical particles. Although it is based on idealized initial conditions, it is widely used for the radiation problems in a light scattering media. This theory mainly calculates the coefficients for absorption, scattering, and extinction. One can find several programs that can perform Mie theory-based solutions. The main advantage of the Mie methods is that they suggest solutions for the cases where the diameter of the scattering particle is comparable with the wavelength of the light. For much larger or smaller particle sizes, there are already several simple methods that can be used in order to describe the behavior of the corresponding systems. Since our focus is on the sizes similar to the incoming light wavelength, we employed the Mie theory calculated spectra to create our database [12, 25]. Our database contains 25 spectra of gold spheres without polymer shell with the diameters 2, 4, 6, …, 50 nm. In Fig. 2, experimental spectra of 5, 7, 10, 15, and 30 nm and their Mie calculated spectra are illustrated. By applying PCA to the whole database, eigenvalues with corresponding eigenvectors of the covariance matrix are obtained. Throughout this work, only the first three eigenvectors, which correspond to the largest three eigenvalues, are considered to reduce the dimension of the initial.

The Mie theory we used in this work employs the spherical vector harmonics to express the electromagnetic fields in the form of scattered shapes for the dipole interactions. Vector-basis functions are derived from the separable solutions to the scalar Helmholtz equation. The relative intensity of the scattering or absorption of particles with different sizes is described by the particle efficiency which is calculated by dividing the scattering/absorption/extinction cross-section by the geometrical cross-sectional area. These cross-sections are obtained by the integration of the Poynting vector for a spherical radius. The experimental size-dependent dielectric electric effects in gold nanoparticles are described by a Drude conduction model. In addition, the enhancement of the local intense fields due to the presence of local surface roughness is described by amplification mechanisms in the model [12, 25].

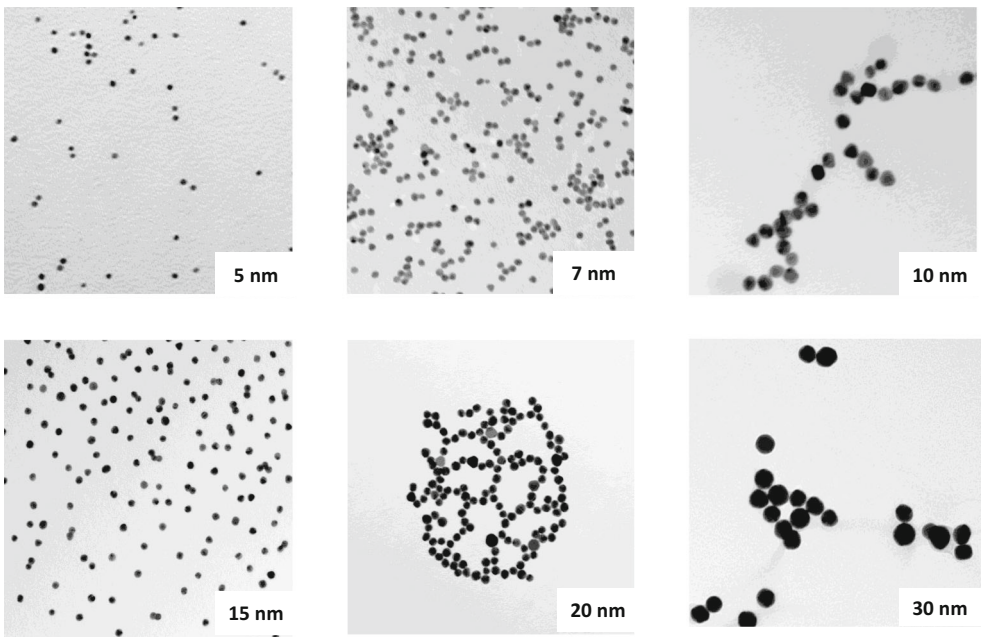

Fig. 1 TEM images of gold nanoparticles

Principal Component Analysis

The goal of PCA is to detect a subspace spanned by the vectors with the greatest variances. This is an optimization problem reducing the dimension of a data set while keeping its variance. It is carried out by transforming the data set of possibly correlated variables to a new set of variables which are called principal components (PC). These PCs are uncorrelated, and they determine the similarities and differences of the data. PCs correspond to the eigenvectors of the covariance matrix which consists of variances of all variables. Therefore, every element of the original data can be stated as a linear combination of PCs. In this paper, the eigenvectors (|PC1>, |PC2>, and |PC3>) which correspond to the first three largest (dominant) eigenvalues of the covariance matrix are considered in order to reduce dimension. In PCA, since the original data is projected into the space spanned by these PCs which are orthonormal, some information is lost due to the eigenvectors corresponding to the small eigenvalues, but this information has less significance [13].

Linear Discriminant Analysis

Similar to PCA, LDA is another dimension reduction technique to identify the hidden structures of large data sets [14]. LDA is applied to data sets, which consist of different classes of similar elements and used to find vectors, to discriminate the classes while respecting the similarities among the class members. Unlike LDA, it deals with the entire data, and it does not consider different classes. Therefore, LDA is applied to data sets when different classes must be considered. The eigenvectors corresponding to the largest three eigenvalues in LDA are |LD1>, |LD2>, and |LD3>.

Artificial Neural Networks

The artificial neural network (ANN) is the most popular and useful method of machine learning algorithms. One of the main features of ANN is the possibility to adapt their behavior to the changing characteristics of the modeled system. As a parallel processing distributed system, ANN depends on learning through a training set of data using a supervised learning algorithm [26]. The processing units in feed-forward and back-propagation neural networks are arranged in multi-layered perceptron (MLP) architectures which have a back-propagation (BP) algorithm and uses various activation functions. The most commonly used non-linear activation functions are the sigmoid and the hyperbolic tangent functions [27, 28]. Other difficulties of deep learning for feed-forward neural networks with multi-layer perceptron are included decision how many numbers of nodes of hidden layers, optimum selection of momentum coefficient, and learning rate [29, 30]. As seen in Fig. 3, each layer of MLP is fully connected to the previous layer and has no other connections. The MLP consists of 3 or more layers including one input, one output, and one or more hidden layers. Multiple hidden layers of non-linearly activating nodes make a deep neural network. In this study, we used four-layered MLP architecture, input and output layers with one node, and hidden layers with five nodes.

The BP with generalized delta learning rule with an iterative gradient algorithm is implemented to minimize the mean square error (MSE) between the actual output of a multi-layered feed-forward neural network and a target output. MSE is also used to measure how well ANN works.

In this study, two different MLP architectures (ANN-1 and ANN2) were used. The architecture of ANN-1 is 1:25:1 which has only 1 hidden layer. The other is 1:5:5:1 which has 2 hidden layers. After trying several numbers of hidden nodes for both MLP architectures, we have selected the optimum number as 25 and 5 respectively. A single input is usually a significant problem in MLP architecture. Moreover, the learning rates and momentum coefficients are chosen to be 0.1 and 0.95 respectively after trying many numbers of coefficients.

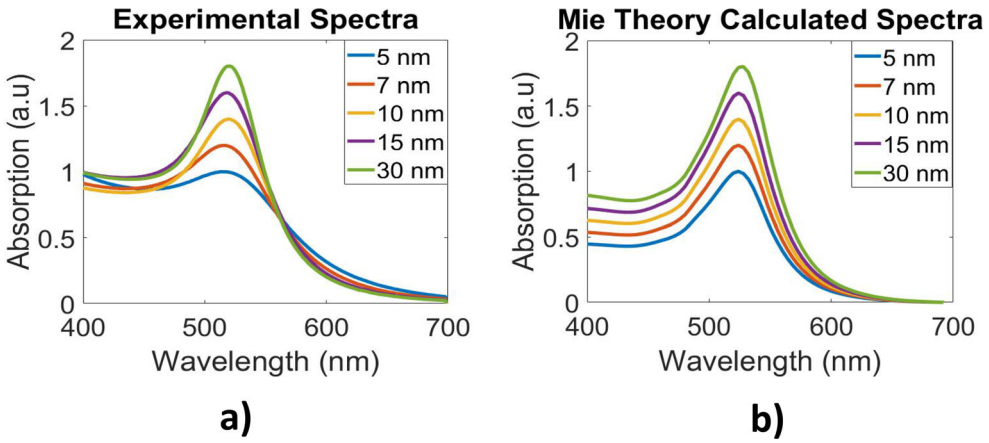

Fig. 2 **a** Experimental UV-Vis spectra and **b** Mie calculated spectra

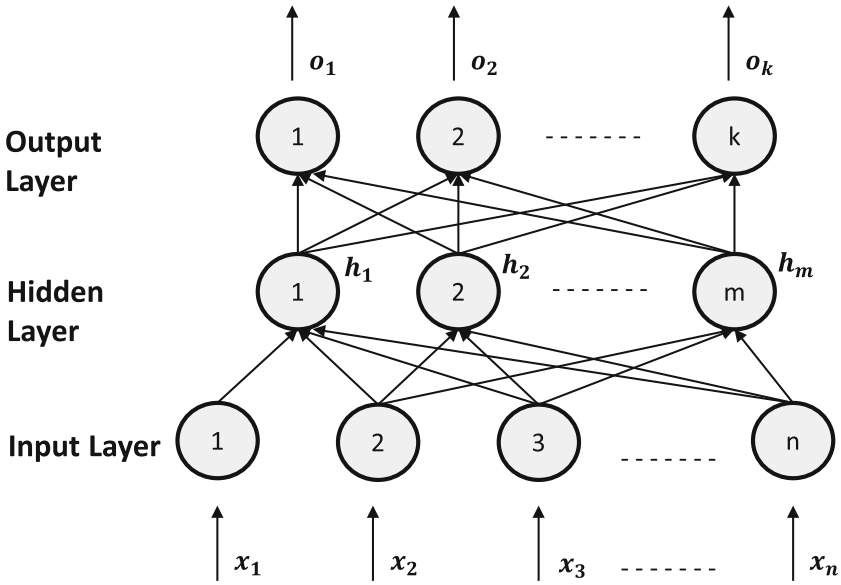

Fig. 3 Illustration of a general MLP architecture

Results and Discussion

Figure 4a illustrates the 3D representation of PCA coordinates of GNS, which exhibits a parabolic profile. Figure 4b illustrates the mean absorbance and vector representation of the spectra. |PC2> vector represents the asymmetric line shape of Fano-like resonance. Fano resonance which results from the interference of the scattering amplitudes of continuous (bright mode) and discrete states (dark mode) provides a field enhancement. It is known that a non-diffractive (airy) beam of surface plasmon polariton (SPP) wave follows a parabolic profile during its travel and Fano resonance originates from the coupling of SPP and waveguide modes [31–34]. Therefore, Fig. 4 shows that PCA can efficiently extract the

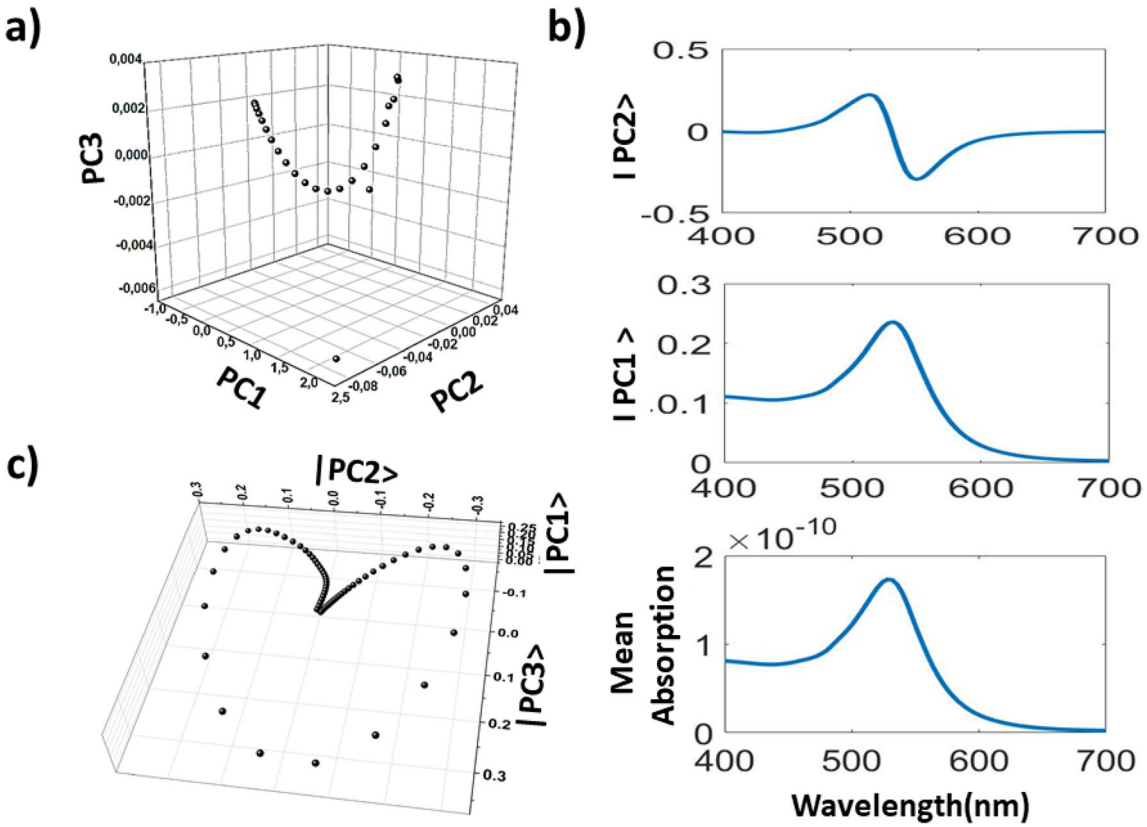

Fig. 4 **a** 3D representation of PC1, PC2, and PC3 coefficients. **b** Spectra of the mean of the initial data, and first two dominant eigenvectors |PC1> and |PC2> of the covariance matrix. **c** 3D vector field of |PC1>, |PC2>, and |PC3>

propagation and resonance characteristics of the SPP over the spectral database of GNS. Furthermore, SPPs are observed in the array and chain form of nanoparticles. Since our database is generated by the spectra of different diameters of gold nanospheres in ascending order, such an array behavior is expected [35].

3D vector spectra plot is given in Fig.4c which represents the homoclinic orbit with a saddle point. The homoclinic orbit is one of the main examples of the occurrence of chaotic strange attractors observed in 3D vector fields (aether) [36]. Such attractors arise under bifurcations of resonant points (fixed saddle point). Luk'Yanchuk et al. stated that Fano resonances from light scattering by nanowires are accompanied by bifurcations of the Poynting vector [37]. Whistler mode plasma waves are also an example of monoclinic orbit attractors generated by stimulated Raman and Brillouin scattering. The process is the conversion of an incident photon into a forward and backscattered photon and ion-acoustic waves (phonons) [38].

In Fig.5a, LDA coordinates in 3D exhibit quantum confinement structure. Such confinements are expected as the size of the particle decreases to nanoscale comparable with the electron's wavelength. The electrons in these structures behave like a particle in a potential well. Confined standing waves are the time-independent solutions of the Schrodinger equations in the potential well which are formed by concurring of two anti-propagating surface plasmon waves [39]. Fig. 5b shows the LDA vector spectra which illustrate the oscillating wave pattern of ion-acoustic waves (|LD1>) and electrons (|LD2>) [14]. Fast Fourier transform modeling of ion-acoustic and electron waves results in oscillation frequency of 31 Hz and 72 Hz, respectively. For reference, typical dust phonon (visible ion-acoustic) waves oscillate around 5–35 Hz [40, 41].

Figure 6a shows that there is a non-linear relation between the extracted PCA and LDA coordinates and the corresponding diameters. PCA coordinates which are obtained from the spectra produced from the Mie scattering theory are used for the training process, and the outputs are the diameters of the nanoparticles. The coordinates of PCA of the Mie calculated spectral database are used for the training of ANN which estimates the diameter of the GNP with high accuracy. In this setting, it should be pointed out that the PCA method provides an advantage for the use of ANN and other machine learning algorithms as it enables the reduction of the dimension of inputs. Since the LDA of spectra of GNSs reveals structures of non-linear ion and electron oscillations (Fig. 6b), LDA-based ANN was not studied in this work.

In Table 1, dynamic light scattering (DLS) measurements of gold spheres and estimations of diameters obtained by ML

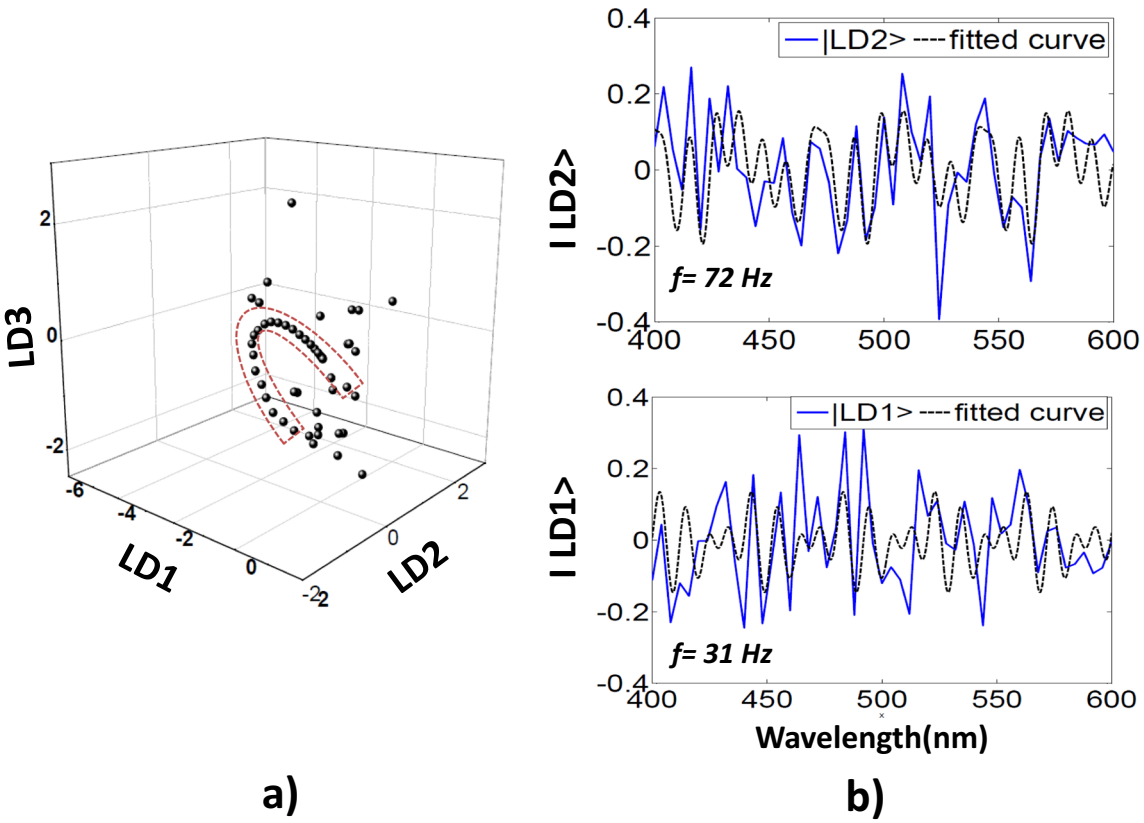

Fig. 5 **a** 3D representation of LD1, LD2, and LD3 coefficients. **b** The spectra of the first two dominant eigenvectors: ion-acoustic (|LD1>) and electron (|LD2>) waves obtained in LDA

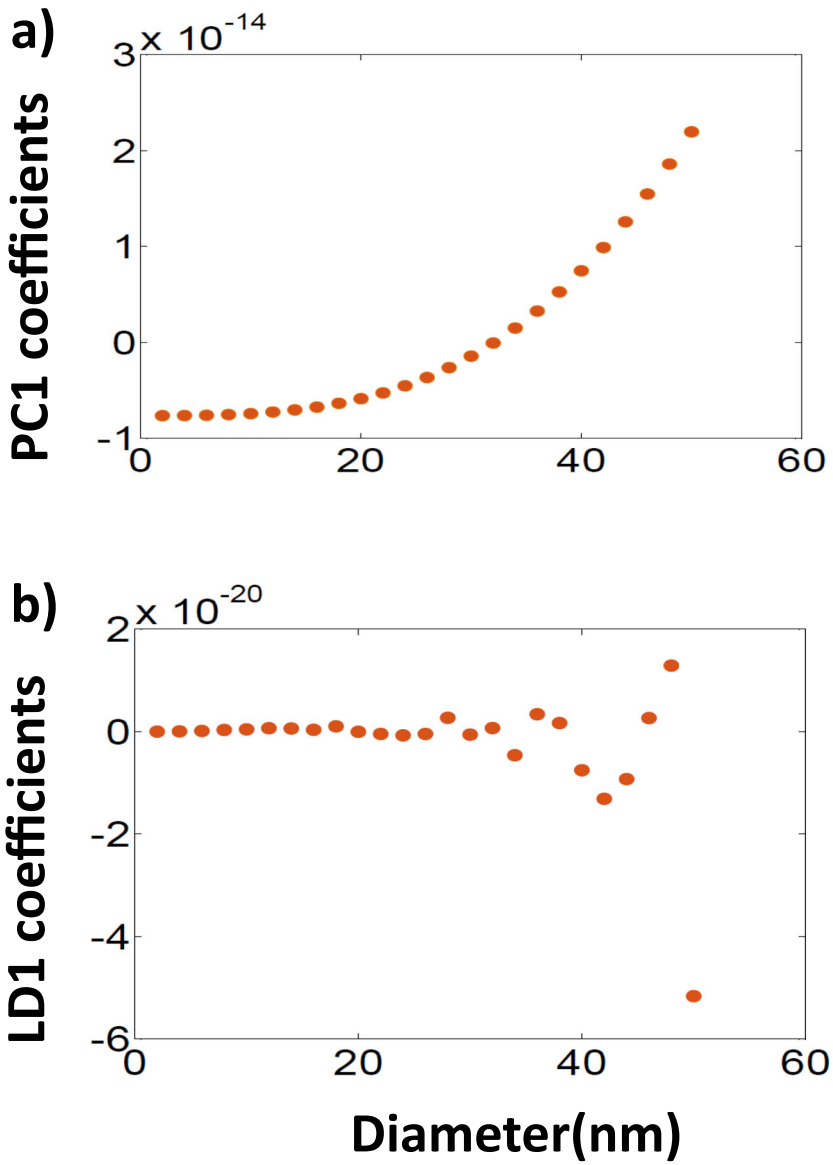

Fig. 6 Plot of **a** |PC1> and **b** |LD1> coordinates versus GNS diameters

algorithms are compared. ANN-2, which consists of (1:5:5:1) MLP structure, has shown the best recognition accuracy which is 100%. Additionally, ANN estimations show that average testing zero error was found for 6 different diameters.

Table 1 Values of measured and estimated diameters with error

NSP (nm)	DLS diameter (nm)	ANN-1 (nm)	ANN-2 (nm)
5	5.0 ± 0.6	7	5
7	7.5 ± 0.8	8	7
10	11.6 ± 1	9	10
15	15.4 ± 1.5	13	15
20	20.5 ± 2.1	20	20
30	31.0 ± 3	30	30
MSE_test_data		1.21	0

It is difficult to estimate 1I1O (one input-1 output) complicated data even if it has small-scale data which has the complex convex region on the data space according to data mining rules. It is also difficult to estimate the spectra for small nanoparticles of different sizes. In this work, we have solved this problem by using multi-hidden-layered ANN as a deep learning algorithm. Deep learning is a class of machine learning algorithms using a cascade of many layers of non-linear processing units for feature extraction and transformation as in ANN-2. Each successive layer uses the output from the previous layer as an input.

In a similar study, Peurifoy et al. have found that test results are better than validation results for the nanoparticular shell 2 and 3, and for the others are the same percentages. These are abnormal results according to ANN because the validation set is different from the test set. The validation set can be

considered a part of the training set because it is used to build the ANN model. However, it is usually used for parameter selection and to avoid overfitting. If the used model is non-linear (like ANN) and trained on a training set only, it will most likely get 100% accuracy which would constitute a case of overfitting and result in poor performance when applied to the test set. Thus, a validation set, which is independent of the training set, is used for parameter selection. In this process, ANN researchers usually use "cross-validation." Moreover, using many nodes for hidden layers is another problem. It causes of longer training time and increased complexity. In addition, our two models both used MLP architectures as 1:25:1 and 1:5:5:1 which are simpler than the MLP architectures which are changing between 1:100:100:1 and 1:250:250:1. The following reasons explain why we have found better results in the more simplest ANN architecture:

1. to use unsupervised PCA for selecting meaningful data set from large data size before ANN classifier.
2. to use better activation function (sigmoid is more effective then rectified linear function).
3. to select the optimum momentum coefficient and learning rate.

Conclusions

Our results show that pattern recognition over UV-vis spectra can provide substantial insights into light-GNS interactions. PCA of the spectral database reveals the Fano resonance characteristics of the SPP. PCA allows us to observe the 3D vector fields(aether) of the spectral data which exhibits the homoclinic strange attractor fixed to resonant saddle points. LDA of spectra reveals the quantum confinement effects, and ion and electron oscillations. Such capabilities show that GNPs have high potentials in high energy density physics and fusion applications besides medical and industrial applications. After the calculation of PCA coordinates, a non-linear relation between the coordinates and the particle diameters is observed. It was due to the PCA coordinates that we could reduce the dimension of input data for the training of ANN, and thereby simplifying the inputs and outputs of ANN modeling.

In this study, we used four well-known and effective ML algorithms and found that the most error-free result came from ANN-2. ANN-2 is, therefore, established as a powerful tool for estimating the diameters with high accuracy, since it resulted in the best recognition accuracy with 100% by using 6 different diameters. In conclusion, a 4-layered ANN model could be suggested as a useful method for predicting the results of a proposed model in terms of saving time and cost, and that pattern recognition–based multi-hidden-layered ANN is a powerful method for estimating the diameters of nanoparticles.

Acknowledgments I would like to express my deepest appreciation to Prof. Abdullah M. Al Rubaish for his support and kindness during my work at Imam Abdul Rahman bin Faisal University, Dammam, KSA. Special thanks to Nanocomposix Inc. for providing TEM images and measurements of nanoparticles and MIE scattering calculator. C.T.Y. acknowledges funds by Nano-Material Technology Development Program of the National Research Foundation of Korea (NRF-2017M3A7B4042140)

References

1. Petryayeva E, Krull UJ (2011) Localized surface plasmon resonance: nanostructures, bioassays and biosensing_A review. Anal Chim Acta 706:8–24
2. Evlyukhin AB, Bozhevolnyi SI, Stepanov AL, Kiyan R, Reinhardt C, Passinger S, Chichkov BN (2007) Focusing and directing of surface plasmon polaritons by curved chains of nanoparticles. Opt Express 15:16667–16680
3. Salandrino A, Christodoulides DN (2010) Airy plasmon: a nondiffracting surface wave. Opt Lett 35:2082–2084
4. Limonov MF, Rybin MV, Poddubny AN, Kivshar YS (2017) Fano resonances in photonics. Nat Photonics 11:543–554
5. DeJarnette D, Norman J, Roper DK (2014) Attribution of Fano resonant features to plasmonic particle size, lattice constant, and dielectric wavenumber in square nanoparticle lattices. Photon Res 2(1):15–23
6. Semouchkina E, Duan R, Semouchkin G, Pandey R (2015) Sensing based on Fano-type resonance response of all-dielectric metamaterials. Sensors. 15:9344–9359
7. Sergeyev SV, Mou C, Turitsyna EG, Rozhin A, Turitsyn SK, Blow K (2014) Spiral attractor created by vector solitons. Light Sci Appl 3(1):e131–e131
8. Kaymak V, Pukhov A, Shlyaptsev VN, Rocca JJ (2016) Nanoscale ultradense Z-pinch formation from laser-irradiated nanowire arrays. Phys Rev Lett 117:035004
9. Ostrikov KK, Beg F, Ng A (2016) Colloquium: nanoplasmas generated by intense radiation. Rev Mod Phys 88:011001
10. Curtis A, Calvi C, Tinsley J, Hollinger R, Kaymak V, Pukhov A, Wang S, Rockwood A, Wang Y, Shlyaptsev VN et al (2018) Micro-scale fusion in dense relativistic nanowire array plasmas. Nat Commun 9:1077
11. Amendola V, Meneghetti M (2009) Size evaluation of gold nanoparticles by UV- vis spectroscopy. J Phys Chem C 113:4277–4285
12. Oldenburg SJ, Averitt RD, Westcott SL, Halas NJ (1998) Nanoengineering of optical resonances. Chem Phys Lett 288: 243–247
13. Yilmaz MF, Danisman Y, Ozdemir M, Karlık B, Larour J (2019) Investigation of electron beam effects on L-shell Mo plasma produced by a compact LC generator using pattern recognition. Matter Radiat Extremes 4:027401
14. Yilmaz MF, Danisman Y, Larour J, Arantchouk L (2019) Linear discriminant analysis based predator-prey analysis of hot electron effects on the X-pinch plasma produced K-shell Aluminum spectra. Sci Rep 9(1):1–8
15. Jackson PC (2019) Introduction to artificial intelligence. Courier Dover Publications, Mineola
16. Yilmaz MF, Eleyan A, Aranchuk LE, Larour J (2014) Spectroscopic analysis of X-pinch plasma produced on the

compact LC-generator of Ecole Polytechnique using artificial neural networks. High Energy Density Phys 12:1–4
17. Wang Q, He H, Li B, Lin H, Zhang Y, Zhang J, Wang Z (2017) UV–Vis and ATR–FTIR spectroscopic investigations of postmortem interval based on the changes in rabbit plasma. PLoS One 12: e0182161
18. Shabanzadeh P, Senu N, Shameli K, Ismail F, Zamanian A, Mohagheghtabar M (2015) Prediction of silver nanoparticles_ diameter in montmorillonite/chitosan bionanocomposites by using artificial neural networks. Res Chem Intermed 41:3275–3287
19. Asadnia M, Khorasani AM, Warkiani ME (2017) An accurate PSO-GA based neural network to model growth of carbon nanotubes. J Nanomater 2017:1–6
20. Peurifoy J, Shen Y, Jing L, Yang Y, Cano-Renteria F, DeLacy BG, Joannopoulos JD, Tegmark M, Soljačić M (2018) Nanophotonic particle simulation and inverse design using artificial neural networks. Sci Adv 4(6):eaar4206
21. Karlik B (2016) The positive effects of fuzzy c-means clustering on supervised learning classifiers. Int J Artif Intell Expert Syst (IJAE) 7(1–8)
22. Turkevich J, Stevenson PC, Hillier J (1951) A study of the nucleation and growth processes in the synthesis of colloidal gold. Discuss Faraday Soc 11:55–75
23. Frens G (1973) Controlled nucleation for the regulation of the particle size in monodisperse gold suspensions. Nat Phys Sci 241(105): 20–22
24. Jana NR, Gearheart L, Murphy CJ (2001) Seeding growth for size control of 5–40 nm diameter gold nanoparticles. Langmuir. 17: 6782–6786
25. Sarkar D, Halas NJ (1997) General vector basis function solution of Maxwell_s equations. Phys Rev E 56:1102–1112
26. Kizilaslan R, Karlik B (2009) Combination of neural networks forecasters for monthly natural gas consumption prediction. Neural Netw World 19(191)
27. Karlik B, Olgac AV (2011) Performance analysis of various activation functions in generalized MLP architectures of neural networks. Int J Artif Intell Expert Syst 1:111–122
28. Karlik B (2003) A neural network image recognition for control of manufacturing plant. Math Comput Appl 8:181–189
29. Glorot X. & Bengio Y. (2010) Understanding the difficulty of training deep feedforward neural networks. In: Proceedings of the thirteenth international conference on artificial intelligence and statistics, pp 249–256
30. Hameed AA, Karlik B, Salman MS (2016) Back-propagation algorithm with variable adaptive momentum. Knowl-Based Syst 114: 79–87
31. Zhu Z, Bai B, You O, Li Q, Fan S (2015) Fano resonance boosted cascaded optical field enhancement in a plasmonic nanoparticle-in-cavity nanoantenna array and its SERS application. Light Sci Appl 4:e296
32. Kong X, Qiu L, Xiao G (2017) Fano resonance in high-permittivity objects. Resonance 189
33. Li L, Li T, Wang SM, Zhang C, Zhu SN (2011) Plasmonic airy beam generated by in-plane diffraction. Phys Rev Lett 107:126804
34. Sekkat Z, Hayashi S, Nesterenko DV, Rahmouni A, Ishitobi H, Inouye Y, Kawata S (2016) Fano resonances arising from coupled surface plasmon polariton and waveguide modes (conference presentation). Plasmonics XIV
35. Jacak WA (2013) On plasmon polariton propagation along metallic nano-chain. Plasmonics. 8:1317–1333
36. Gonchenko SV, Ovsyannikov II (2015) Homoclinic tangencies to resonant saddles and discrete Lorenz attractors. arXiv preprint arXiv 1509:00264
37. Luk'Yanchuk BS, Miroshnichenko AE, Kivshar YS (2013) Fano resonances and topological optics: an interplay of far-and near-field interference phenomena. J Opt 5(7):073001
38. Sharma RP, Rozmus W, Offenberger AA (1986) Stimulated Brillouin scattering of whistler waves off the kinetic Alfvén waves in plasmas. Phys Fluids 29(12):4055–4059
39. Crommie MF, Lutz CP, Eigler DM (1993) Confinement of electrons to quantum corrals on a metal surface. Science. 262:218–220
40. Merlino RL (2009) Dust-acoustic waves: visible sound waves. AIP Conf Proc 1188(1):141–152
41. Mendonça JT, Rao NN, Guerreiro A (2001) Chargeons and phonons in a dusty plasma. EPL (Europhys Lett) 54(6):741